9th AIAA Aviation Technology, Integration, and Operations Conference (ATIO)
and
Air
21 - 23 September 2009, Hilton Head, South Carolina

AIAA 2009-6983

An Operational Strategy for Persistent Contrail Mitigation

Scot E. Campbell[1], Natasha A. Neogi[2], and Michael B. Bragg[3]
University of Illinois Urbana-Champaign, Urbana, IL, 61801

The formation of persistent contrails has been recognized as a potential threat to the global climate. This paper presents a methodology to optimally reroute aircraft trajectories to mitigate the formation of persistent contrails with the use of mixed integer linear programming (MILP). The path planning algorithm was developed so that flights through areas conducive to persistent contrail formation are assessed a penalty which can be adjusted by the user before the flight. The tradeoff between persistent contrail formation and increased fuel burn was analyzed for flights of different contrail formation penalty weighting. It was found that fuel burn increased 1.48% when approximately 50% of persistent contrails were avoided and 6.19% when 100% of persistent contrails were avoided.

I. Introduction

Air transportation is critical to the world's infrastructure, economy, and quality of life. Increasing demand for air travel has pushed the utilization of the air traffic system to its limits, manifesting itself in a loss of efficiency, degradation of flight safety, and increased environmental impact. Aviation affects the environment in many ways including land use, noise pollution, local air quality, and climate.[1] Although its effect on climate is currently not fully understood,[1] there are well founded concerns that aircraft emissions might play a larger role in future global climate change.[2,3] The three largest aviation emissions effectors on the climate are direct emission of greenhouse gases such as CO_2, emissions of NOx, and persistent contrails.[2,3] In general, persistent contrails are formed when an aircraft passes through an ice-supersaturated region in the atmosphere. Although the complete effect of persistent contrails on the environment is not known, there is evidence to suggest an effect,[4] and it is predicted that persistent contrails have a three to four times greater effect on the climate than CO_2 emissions.[1] With a projected three fold increase in air traffic by the year 2025,[5] the effect of aviation on the environment will increase with time. Recent research has investigated operational strategies to mitigate persistent contrail formation through air traffic management scenarios. These strategies include the restriction of cruise altitudes,[6-8] the real-time adjustment of cruise altitude,[9] and rerouting the flight plans of aircraft to avoid areas conducive to persistent contrail formation.[10] In addition, an optimal strategy for contrail avoidance was proposed, but this strategy precluded any flight through a region conducive to contrail formation, which is not ideal from an operational standpoint.[11] This research builds upon the optimal contrail avoidance strategy to include the capability to penetrate areas conducive to persistent contrail formation, where flight would be penalized instead of precluded.

Optimal trajectory planning has been investigated through many different techniques.[12-16] Mixed-integer programming (MILP) has been successfully applied to trajectory optimization problems involving constrained dynamics and obstacle avoidance using both full horizon, and receding horizon implementations.[15-22] One drawback to full horizon MILP is the optimization can be intractable for large problems, i.e. many obstacles, discrete time steps, dynamic constraints. To make large problems tractable, a receding horizon controller can be used to speed up the solution time.[17,18] A receding horizon controller essentially finds the optimal trajectory up to a certain point, called the planning horizon, and then approximates the remaining trajectory to the goal.[17] The controller executes a pre-specified number of time steps in the optimal trajectory and the optimization is iterated until the goal is reachable in the planning horizon.[17] This paper will use MILP to find the fuel optimal trajectory of an aircraft flying from O'Hare International Airport (KORD) to Los Angeles International Airport (KLAX) while mitigating persistent contrail formation.

[1] Graduate Research Assistant, Aerospace Engineering, AIAA Member.
[2] Assistant Professor, Aerospace Engineering, AIAA Member.
[3] Professor, Aerospace Engineering, Executive Associate Dean for Academic Affairs, AIAA Fellow.

II. Contrail Formation and the Atmospheric Model

Contrails are line-shaped clouds that form behind aircraft at high-altitudes.[23] After forming, contrails dissipate if the relative humidity with respect to ice (RHi) is low, and persist if the RHi is high. The RHi threshold at which contrails persist is thought to vary between 95-105%,[24] but for simplicity, this paper used RHi > 100% to define the necessary condition for persistent contrail formation.

Regions of ice supersaturation (RHi > 100%) typically develop in areas of rising air motion and are defined by boundaries on the order of 150 km horizontally[26] and approximately 500 m vertically.[27] Currently, there is not an accurate forecast model to predict areas of ice supersaturation, and it is difficult to measure relative humidity at altitudes near cruise,[25] however, fields of RHi can be estimated with the following tools.

Tools such as the Microwave Limb Sounder (MLS) and the Atmospheric Infrared Sounder (AIRS) have been used to detect areas of supersaturation.[28,29] Unfortunately, the data available from these tools has poor vertical resolution of the ice supersaturation in the region. The MOZAIC program collected 9 years of data along major flight routes, however these data do not include off-route measurements.[30] In addition, satellites have been used to detect contrail formation but not explicitly areas of supersaturation. Forecast models for relative humidity include The European Center for Medium-Range Weather Forecasts (ECMWF)[31] and the Rapid Update Cycle (RUC). The RUC is an atmospheric prediction system that is principally a numerical forecast model developed for users needing short-range weather forecasts.[32] This paper used RUC data with a horizontal resolution of 20km. The vertical resolution of these data are isobaric pressure levels ranging from 100-1000mb in 25mb increments.

This paper used archived RUC data from November 17, 2001. Figure 1 shows the November 17, 2001 field of RHi at different times. The red areas indicate RHi greater than 100% in the region. During the time period of 1700Z-2000Z the RHi field did not change significantly, which is typical.

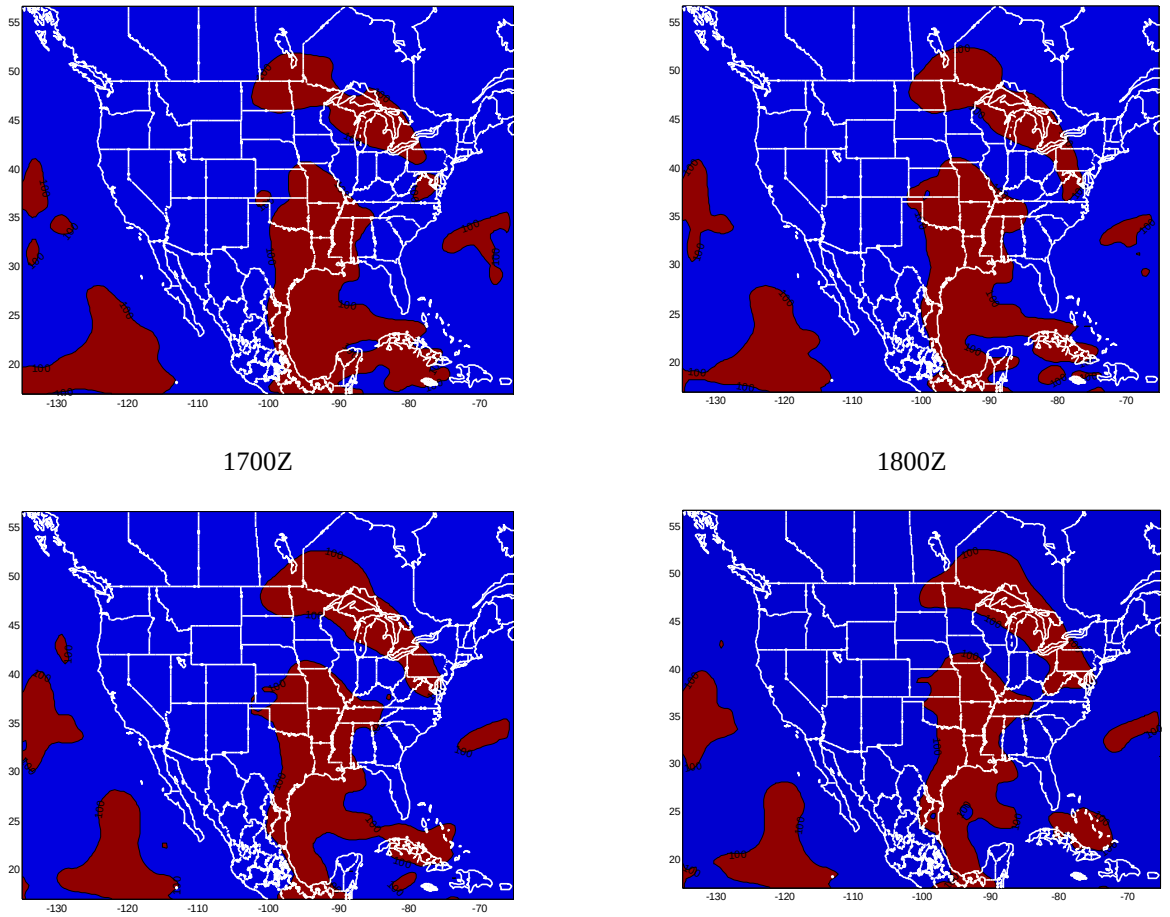

Fig. 1 Fields of RHi at Different Times on November 17, 2001, RUC data.

Also, it should be noted that the size of the RHi fields change with altitude. For MILP implementation, the areas of RHi > 100% were represented as overlapping cuboids.

It should be understood that while the RHi estimates from the RUC data are representative of areas of supersaturation, the values of RHi in the estimates are biased. This is a result of dry bias in some radiosonde measurements that are used in the model. Therefore, the assumption is that even though the RHi fields might not be accurate, they are representative enough that a path planning tool can be developed and successfully applied to more accurate data when it comes available.

III. Aircraft Fuel Burn Model

Aircraft fuel burn is a complicated quantity that is dependent on many states and aircraft-specific parameters. In practice, fuel burn is predicted based on flight test data taken over a wide range of operating conditions. In lieu of these data, fuel burn can be approximated with a limited set of aircraft and engine data. Previous studies have predicted fuel burn using the FAA's System for Assessing Global Emissions (SAGE),[10] a modified version of SAGE,[33] and a quadratic approximation based on velocity.[34] Existing work using the MILP framework have approximated fuel burn by the 1-norm of the aircraft acceleration.[20,21] This paper uses aircraft data and engine performance simulation software to approximate fuel burn over the cruise flight envelope. This method is better model than a 1-norm approximation or velocity approximation, but simple enough to implement in the mixed-integer programming framework.

A. Aircraft Performance

The aircraft performance model used for this paper was created to emulate the en-route performance characteristics of medium-range aircraft such as the Boeing 737 and Airbus A320. The following restrictions were placed on the altitude and Mach number to confine aircraft performance to the cruise envelope, as seen in Eq. (1)

$$\begin{aligned} 0.70 \le M \le 0.82 \\ 28{,}000\, ft \le z \le 42{,}000\, ft \end{aligned} \tag{1}$$

where M is the Mach number and z is the altitude. To compute the performance, the drag coefficient was extracted from drag polar data[35] for a range of Mach numbers, altitudes, and weights. The thrust required was calculated for the range of Mach numbers and altitudes given by Eq. (1) and for three weights, each representing the aircraft weight at a different fuel state along the flight path.

B. Engine Performance

Engine performance was obtained with the Engine Performance Analysis Program v4.2.[36] This program used a set of engine parameter inputs and flight conditions (Mach number, altitude) to compute curves of thrust specific fuel consumption (TSFC) vs. engine thrust. The engine was assumed to be a high-bypass turbofan, and the software input parameters are given in Table 1.

Table 1 Engine Performance Software Input Parameters

Mass Flow Rate (max throttle, sea level)	779 lbm/sec
Bypass Ratio	5.1
Compressor Pressure Ratio	32.8
Fan Pressure Ratio	2.3

The program was run for the range of Mach numbers and altitudes given by Eq. (1). The engine performance data were tabulated for use in the aircraft fuel burn model.

C. Aircraft Fuel Burn

Aircraft fuel burn was calculated for a range of Mach numbers, altitudes, and weights using Eq. (2)

$$W_f = T_{req} \cdot TSFC \tag{2}$$

where W_f is the fuel flow, T_{req} was found by the aircraft performance calculations, and $TSFC$ was found by the engine performance model. Figures 2 and 3 show the relationship of altitude and velocity with fuel flow, respectively, for an aircraft weight of 145,000 lb with engine and drag characteristics described above.

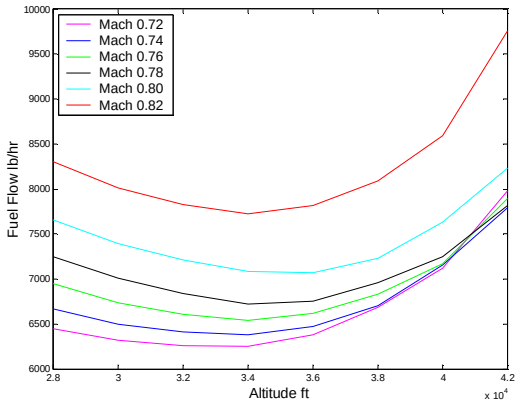

Fig 2. Altitude vs. Fuel Flow for W = 145,000 lb

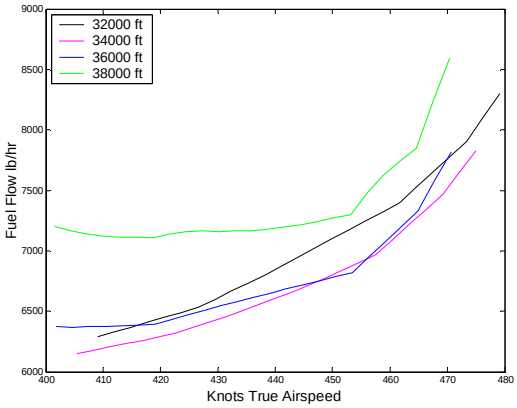

Fig 3. Velocity vs. Fuel Flow for W = 145,000 lb

Figures 3 and 4 show the highly nonlinear nature of fuel burn. To simplify this behavior, a nominal flight condition was selected (Mach number, altitude) for a given weight, and the change in fuel burn around the nominal flight condition was modeled. The nominal cruise Mach number was selected to be 0.78 based on typical cruise speeds for the type of aircraft considered in this model.[38] The nominal cruise altitude was selected based on the optimal altitude for a Mach number of 0.78 and for a given weight. Ideally, the nominal altitude would increase continuously as the weight of fuel is burned off of the aircraft, resulting in a cruise climb flight profile. However, this procedure is generally not performed in practice because of air traffic control restrictions. Instead, a step-climb procedure is used, where the altitude is increased in discrete steps along the flight path.[39] This model emulated a step climb by using three nominal cruise altitudes based on the optimal altitude for three aircraft weights. The initial weight was assumed to be 145,000 lbs, and the subsequent weights were 135,000 lbs and 125,000 lbs, which corresponded to optimal altitudes of approximately 34,000 ft, 36,000 ft, and 38,000 ft, respectively, for a Mach number of 0.78. Table 3 gives the nominal flight conditions used for this model.

Table 2 Nominal Flight Conditions

Weight (lb)	Altitude (ft)	Mach number	True airspeed (knots)
145,000	34,000	0.78	451
135,000	36,000	0.78	447
125,000	38,000	0.78	447

Figures 4 and 5 show the sensitivity of fuel flow to changes in altitude and velocity around the nominal flight conditions, respectively.

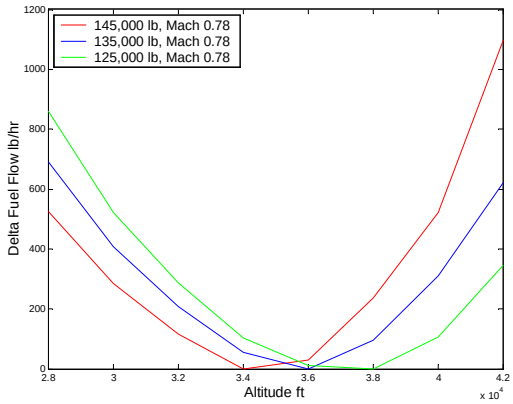

Fig. 4 Sensitivity of fuel flow to altitude

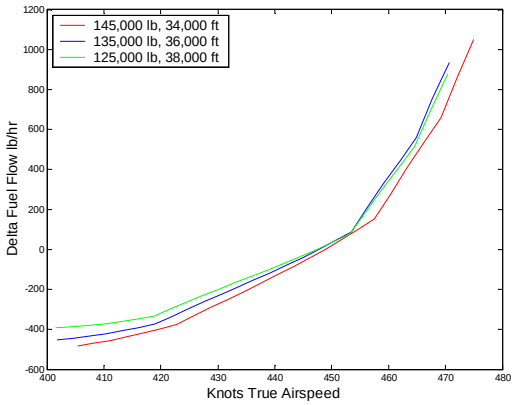

Fig. 5 Sensitivity of fuel flow to velocity

IV. Path Planning Algorithm

This section describes the formulation of the persistent contrail mitigation problem as a receding horizon mixed-integer linear program (RH-MILP). The receding horizon controller can be thought of in two parts: a detailed trajectory optimization with a pre-specified time horizon, followed by a less refined approximation of the cost from the end of the detailed trajectory to the goal. Once the detailed trajectory and approximate cost-to-go is optimized, a pre-specified number of time steps in the detailed trajectory are executed, and the optimization is recomputed with the updated initial condition. This procedure continues until the goal is reachable in the time horizon of the detailed trajectory, also called the planning horizon. Existing research using RH-MILP for path planning has represented obstacles with hard avoidance constraints, which do not allow a path through the obstacle.[11,16,17] This paper presents a new RH-MILP formulation that employs soft constraint to allow flight through an obstacle with a penalty in the cost function. The optimizations were solved using CPLEX[40] 10.2 on a laptop with a 2.16 GHz Intel Core2 Duo processor and 2 GB of RAM.

A. Aircraft Dynamical and Performance Constraints

The detailed trajectory optimization phase of the receding horizon controller uses MILP to find the fuel optimal trajectory from an initial state to the end of the planning horizon. This aircraft model is based upon existing research.[11]

The dynamical constraints presented here are that of a double integrator and the evolution of the aircraft states is governed by Eq. (3)

$$\mathbf{x}(k+1) = A\mathbf{x}(k) + b\mathbf{u}(k) \tag{3}$$

where,

$$\mathbf{x} = \begin{bmatrix} x \\ y \\ z \\ v_x \\ v_y \\ v_z \end{bmatrix} \qquad \mathbf{u} = \begin{bmatrix} a_x \\ a_y \\ a_z \end{bmatrix} \qquad A = \begin{bmatrix} I_3 & \Delta t \cdot I_3 \\ 0_3 & I_3 \end{bmatrix} \qquad b = \begin{bmatrix} \frac{1}{2}\Delta t^2 \cdot I_3 \\ \Delta t \cdot I_3 \end{bmatrix} \tag{4}$$

The vector **x** represents the position and velocity of the aircraft, the vector **u** represents the acceleration, k is the discrete time step, and Δt is the size of the time step.

The calculation of velocity magnitude from the individual velocity components requires the square root of the sum of the squares, which is obviously a nonlinear operation and inadmissible in MILP. Therefore an accurate method is needed to approximate the magnitude of velocity because fuel burn is largely dependent on the speed of

the aircraft. The following procedure provides a linear approximation of the velocity and the acceleration for implementation into the MILP[16]

$$V[k] \geq v_x[k]\cos\left(\frac{2\pi m}{M}\right) + v_y[k]\sin\left(\frac{2\pi m}{M}\right) \tag{5}$$

$$V[k] - R\cdot(1-b_v[k,m]) \leq \left(v_x[k]\cos\left(\frac{2\pi m}{M}\right) + v_y[k]\sin\left(\frac{2\pi m}{M}\right)\right)\cdot 1.01 \tag{6}$$

$$A[k] \geq a_x[k]\cos\left(\frac{2\pi m}{M}\right) + a_y[k]\sin\left(\frac{2\pi m}{M}\right) \tag{7}$$

where V and A are the velocity and acceleration magnitudes respectively, b_v is a binary variable, R is a large constant, and m is an integer in the set of integers from 1 to M. Equation 6 is necessary to include non-convex constraints on minimum velocity. It should be noted here that the velocity and acceleration magnitude approximations only account for motion in the x-y direction. Motion in the z-direction was treated separately. Additionally, V and A were bounded to constrain the optimization within a realistic flight envelope, as given in Eqs. (8) and (9):

$$V_{\min} \leq V \leq V_{\max} \tag{8}$$

$$A \leq A_{\max} \tag{9}$$

The vertical velocity was constrained by a rate of climb limit, which was a function of the altitude. The maximum rate of climb was defined by Eq. (10)

$$RC_{\max} + \beta_1 z = \beta_0 \tag{10}$$

where RC_{max} is the maximum rate of climb, and β_i was computed in the aircraft model. The rate of climb was constrained by the maximum rate of climb using Eq. (11)

$$v_z - RC_{\max} \leq 0 \tag{11}$$

The maximum descent rate was represented by a lower bound on the vertical velocity and was chosen to be a value consistent with normal operation of commercial aircraft.[36]

Terminal constraints were used to encourage the aircraft to reach the goal if the goal was reachable in the planning horizon. These constraints use binary variables and are shown in Eqs. (12) and (13)

$$\begin{aligned}
x[k] + R\cdot b_f[k] &\leq R + x_f \\
x[k] + R\cdot b_f[k] &\leq R - x_f \\
y[k] + R\cdot b_f[k] &\leq R + y_f \\
y[k] + R\cdot b_f[k] &\leq R - y_f \\
z[k] + R\cdot b_f[k] &\leq R + z_f \\
z[k] + R\cdot b_f[k] &\leq R - z_f
\end{aligned} \tag{12}$$

$$\sum_{i=1}^{N_p} b_f[i] \leq 1 \tag{13}$$

where $b_f[k]$ is the binary variable corresponding to time step k, (x_f, y_f, z_f) is the final position, and R is a large constant used to relax the constraint. In the literature, this approach is referred to as the "big-M" approach.

B. Contrail Mitigation Constraints

Contrail mitigation is accomplished within the MILP framework by defining areas conducive to contrail formation as cuboids, and then penalizing flight through these regions, which is solvable by mixed-integer linear programming. Equations 14 and 15 show the constraints used to penalize persistent contrail formation.

$$\begin{aligned} x[k] &\leq C_{x,low} + R \cdot b_{o,1}[k] \\ x[k] &\geq C_{x,high} - R \cdot b_{o,2}[k] \\ y[k] &\leq C_{y,low} + R \cdot b_{o,3}[k] \\ y[k] &\geq C_{y,high} - R \cdot b_{o,4}[k] \\ z[k] &\leq C_{z,low} + R \cdot b_{o,5}[k] \\ z[k] &\geq C_{z,high} - R \cdot b_{o,6}[k] \end{aligned} \tag{14}$$

$$\sum_{i=1}^{6} b_{o,i}[k] \leq 5 + g[k] \tag{15}$$

The variable C defines the 6 planes that compose the cuboid which represents an area of RHi > 100%. The variable $b_{o,i}$ is a binary variable that is either 1 or 0 depending on whether constraint i is active, and g is a binary variable that takes the value 1 when all 6 constraints are active. This variable is weighted in the cost function and assigns a penalty to contrail formation.

C. Detailed Trajectory Cost Function

The fuel burn was modeled in a piecewise-linear fashion as was presented in section III, and the effect of Mach number, altitude, and throttle setting were assumed to be decoupled around a nominal flight condition and weight. Also, the effect of weight was accounted for by changing the nominal flight condition at pre-specified intervals of time, corresponding to the approximate time the aircraft becomes 135,000 lbs and 125,000 lbs during the flight. The fuel burn curves given in Figs. 4 and 5 were written as a set of piecewise linear functions. The piecewise linear representation of fuel burn as a function of weight is described by Eqs. (16) and (17):

$$f_a(W) = \max(\propto_1 z + \propto_2, ..., \propto_i z + \propto_{i+1}) \quad \text{for } i = 1,3,5,\ldots \tag{16}$$

$$f_v(W) = \max(\sigma_1 V + \sigma_2, ..., \sigma_i V + \sigma_{i+1}) \quad \text{for } i = 1,3,5,\ldots \tag{17}$$

where $f_a(W)$ and $f_v(W)$ are the fuel burn associated with altitude and velocity, respectively, W is weight, and μ_i and σ_i determine the piecewise linear function. These equations are written in MILP format as follows:

$$\begin{aligned} &\propto_1 z - f_a \leq \propto_2 \\ &\quad \vdots \qquad\qquad \text{for } i = 1,3,5,\ldots \\ &\propto_i z - f_a \leq \propto_{i+1} \end{aligned} \tag{18}$$

$$\begin{aligned} \sigma_1 V - f_v &\le \sigma_2 \\ &\vdots \qquad\qquad \text{for } i = 1,3,5,\ldots \\ \sigma_i V - f_v &\le \sigma_{i+1} \end{aligned} \tag{19}$$

It should be noted that the coefficients μ and σ depend on the aircraft weight; therefore these equations are updated whenever the aircraft weight is updated.

The effect of climb and descent on fuel burn was assumed to be decoupled from the effects of velocity, altitude, and weight. During cruise, commercial aircraft frequently change altitude using the flight level change mode of the flight management system, and therefore it was assumed that the thrust is set to maximum climb thrust during climb, and idle during descent. The climb and descent state was characterized with Eq. (20)

$$\begin{aligned} v_z &\le R \cdot b_{climb} \\ -v_z &\le R \cdot b_{descend} \end{aligned} \tag{20}$$

where v_z is the vertical velocity, R is a large constant, b_{climb} is a binary variable to indicate climb, and $b_{descend}$ is a binary variable to indicate descent.

The last component of the cost is the fuel burn associated with acceleration, which is determined under the assumption that the fuel burn linearly increases with acceleration. In full, the cost function for the detailed trajectory optimization is written as Eq. (21)

$$J = \left(f_a + f_v + A\right)\Delta t - \sum_{i=1}^{N_p} b_{f,i} f_{term,i} + b_{climb,i} f_{descend} + b_{descend,i} f_{descend} + g_i \cdot P_{contrail} \tag{21}$$

where f_a and f_v are the fuel cost associated with altitude and velocity, respectively, A is acceleration, f_{climb} is a weighting associated with maximum climb thrust, $f_{descend}$ is a weighting associated with idle, Δt is the time step, and $P_{contrail}$ is a weighting applied to the contrail penalty. Again, it should be noted that f_a and f_v change with aircraft weight, which is updated periodically during the receding horizon optimization.

D. Algorithm Overview

As stated previously, the optimization approach used in this research can be described by two parts of different resolution: the near term and the far term. In the near term the trajectory is optimized at a relatively high resolution of waypoints and subject to more computationally demanding constraints. In the far term the optimal trajectory is approximated using a coarse resolution of waypoints to reduce the computational burden of the problem. Generally speaking, the waypoints in the near term are called the planning horizon and the waypoints in the far term are called the cost to go. After a predetermined number of waypoints are executed in the planning horizon, the trajectory in the near term is updated based on a new initial position and the optimization iterates until the aircraft reaches the destination. The steps of the optimization procedure are as follows:

1. Find nominal trajectory disregarding persistent contrail formation

This trajectory is solved using the same MILP framework as before, except the trajectory is in absence of obstacles and a receding horizon controller is not needed because of the extreme reduction of binary variables due to the exclusion of obstacles. The nominal trajectory is used in the cost-to-go function to assist the receding horizon controller in following an optimal trajectory.

2. Create cost grid relative to the aircraft initial position

A cost grid was created to represent the far-field of the receding horizon controller. The grid consisted of a set of nodes extending radially outward from the aircraft. Figure 6 shows a top-down view of the cost grid. It is important to keep in mind that the cost grid is 3-dimensional, and Fig. 6 only shows one layer of the grid. The nodes (black dots in Fig. 6) lie outside of the space reachable by the aircraft in the planning horizon and were defined by the following equations:

$$r_0 = V_{\max} \cdot N_p \cdot \Delta t \tag{22}$$

$$x_{i,j} = (r_0 + \delta_i)\sin\theta_j \tag{23}$$

$$y_{i,j} = (r_0 + \delta_i)\cos\theta_j \tag{24}$$

$$\delta_{i+1} = \delta_i + i \cdot \varepsilon \tag{25}$$

$$\theta = \{\theta_1, \ldots, \theta_n\} \text{ for } i = 1 \ldots n \tag{26}$$

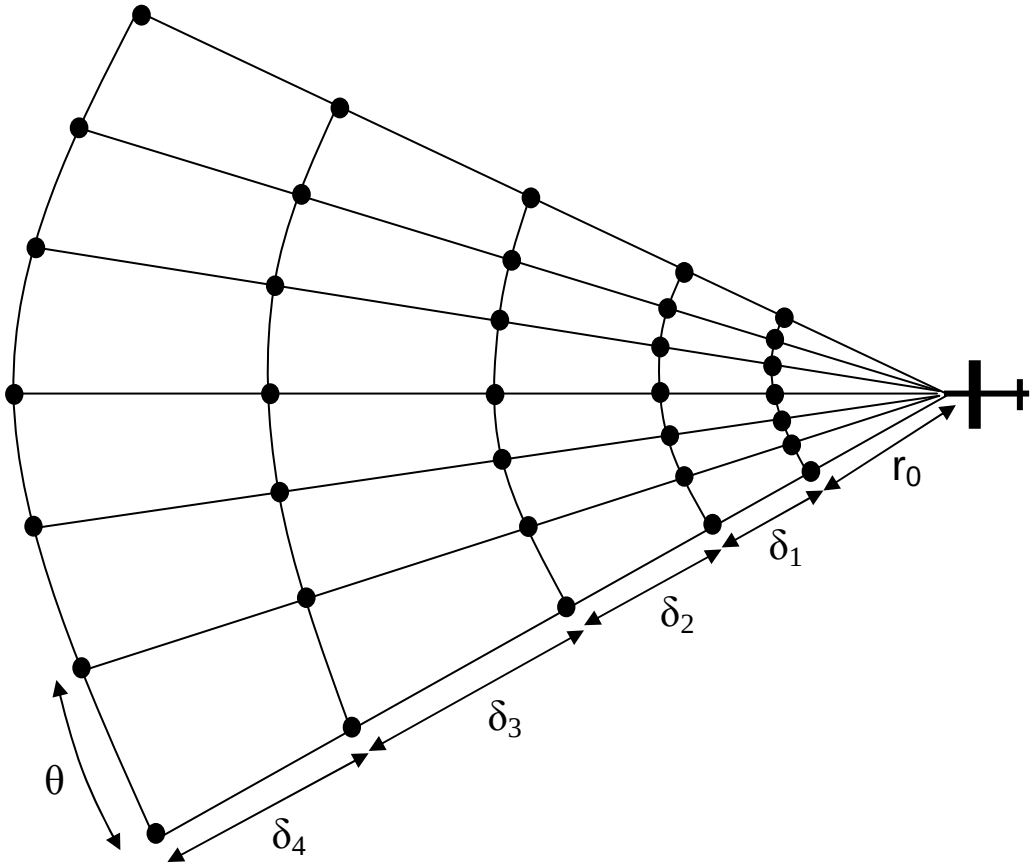

Fig 6. Cost Grid Representation

where V_{max} is maximum velocity, N_p is the number of steps in the planning horizon, Δt is the size of the time step, and ε is a constant. A cost was assigned to each node and the grid of nodes was used to find the cost-to-go of the receding horizon controller.

3. Populate cost grid and create visibility graph

Each node in the cost grid was assigned a penalty value based on it's altitude, distance from the nominal trajectory found in step 1, and whether or not the node lies in an area of ice supersaturation. The cost-to-go in the receding horizon controller was found using a modified version of Dijkstra's algorithm, which takes into account not only the distance between nodes, but also the penalty value assigned to the node.

4. Find path of least cost using a modified Dijkstra's algorithm

This path connects the first row of nodes in the cost grid (located distance r_0 from the aircraft) to the destination. The cost-to-go trajectory passes though the nodes corresponding to the path of least cost.

5. Find optimal trajectory mitigating persistent contrail formation and update initial position

The detailed trajectory segment of the receding horizon controller was optimized according to dynamical constraints and performance limits consistent with a medium size jet transport aircraft. The end of the detailed trajectory was connected to the first row of nodes in the cost grid with the line of sight method used previously.[59] As mentioned before, the trajectory was optimized with RH-MILP.

6. Repeat until the destination is reached

The number of iterations of the optimization is dependent on the distance between the origin and destination, the time step size, and the number of waypoints in the execution horizon.

V. Results

This example considers a single flight from O'Hare International Airport (ORD) to Los Angeles International Airport (LAX) using atmospheric data from November 17, 2001. The objective of this example was to find a fuel optimal trajectory for this route while flying clear of atmospheric areas containing RHi > 100%. The fuel burn cost was derived from the model presented in Section III, and the formulations of Sections IV describe the dynamical and aircraft performance constraints. Table 3 lists the receding horizon parameters and the aircraft performance limitations used in this example.

Table 3 Receding horizon parameters and aircraft performance limits

Number of steps in planning horizon (N_p)	12
Number of steps in the execution horizon (N_e)	6
Time step size (Δt)	3 min
Maximum en-route velocity (V_{max})	470 knots
Minimum en-route velocity (V_{min})	417 knots
Maximum altitude (z_{max})	42,000 ft
Minimum altitude (z_{min})	28,000 ft

Figure 7 shows trajectories overlaid on two-dimensional contour plots of the RHi field at different altitudes. The blue, black, and red trajectories correspond to optimizations with 100%, 50%, and 0% contrail mitigation, respectively. The trajectories were initiated at approximately 34,000 ft, it should be noted that the red and black trajectories are overlaid on each other in Figure 7. The 0% and 50% contrail mitigation trajectories follow an almost identical straight line trajectory from ORD to LAX with the only difference being in the altitude. The 100% contrail mitigation trajectory was forced to adjust its horizontal flight path in addition to its altitude to avoid flight into an area of RHi > 100%.

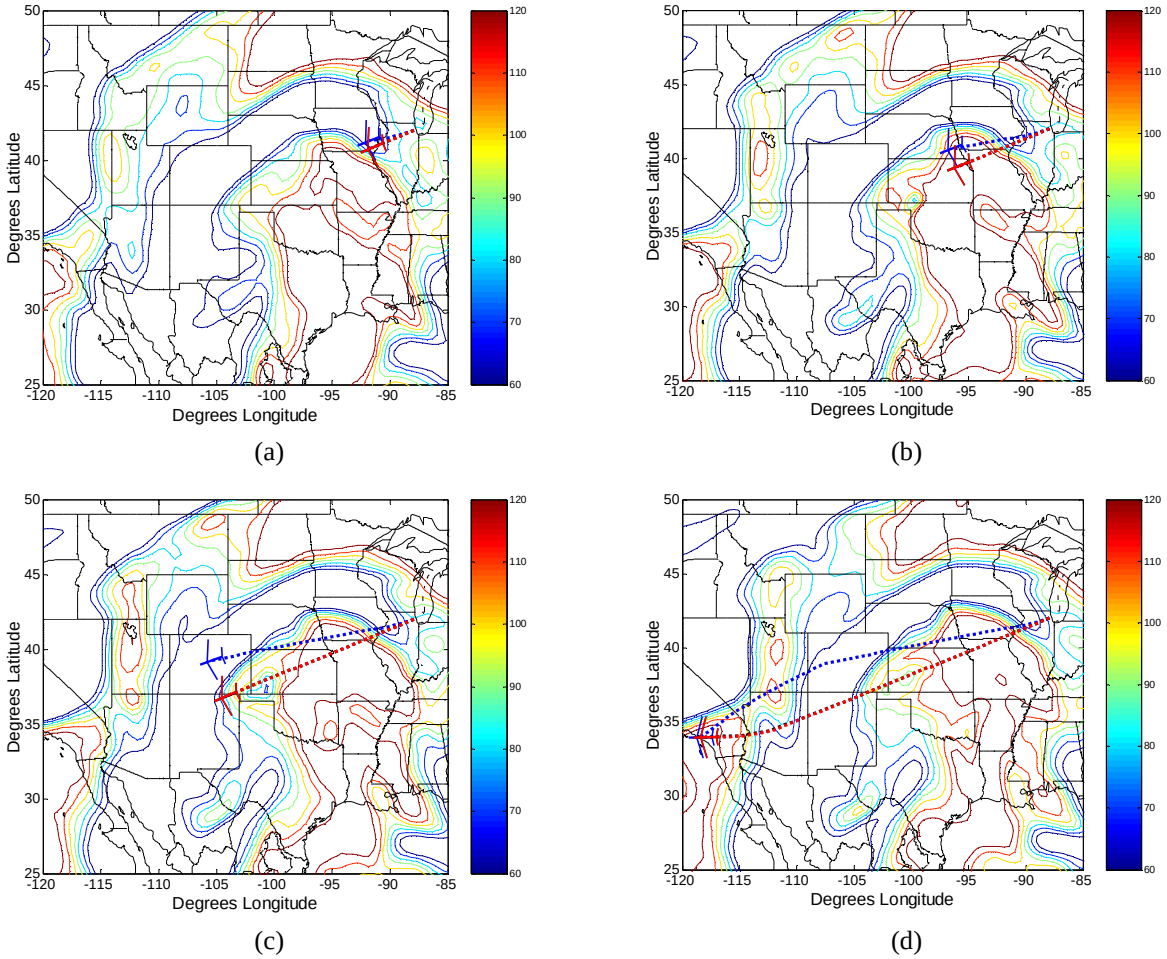

Fig. 7 Fuel optimal trajectories overlaid on contour plots of the RHi field at times of (a) 1730Z, (b) 1800Z, (c) 1900Z, and (d) 1940Z. A map showing the boundaries of North America is in the background.

Figure 8 shows the aircraft and contrail mitigation performance associated with the trajectories presented in Fig. 7. Figure 8a shows the velocity profiles of the trajectories, and it is easy to see that the Mach numbers of the 0% and 50% trajectories (red and black respectively) remain constant at roughly 0.78. On the other hand, due to a longer flight path the 100% trajectory (shown in blue) increases its Mach number in an attempt to arrive in LAX at the same time as the 0% trajectory. Figure 8b shows the altitude profiles of the trajectories. The 0% trajectory does not change its altitude to avoid contrail formation. The altitude increases on the 0% trajectory because the nominal flight condition changes for the step climb procedure. The 50% and 100% trajectories have the same nominal flight condition as the 0% but adjust their altitude to fly either above or under areas of RHi > 100%. The persistent contrail length produced by each trajectory was normalized by the straight line distance between ORD and LAX. This normalized contrail length was 0.42 for the 0% trajectory, 0.22 for the 50% trajectory, and 0.0 for the 100% trajectory.

Table 4 compares the performance of the three trajectories presented by this example. The trajectory with 100% contrail penalty avoided producing any persistent contrails, but it consumed significantly more fuel than the other two trajectories. The 50% contrail penalty trajectory mitigated contrail formation by almost 50% by altering its altitude and only had a slight increase in fuel burn.

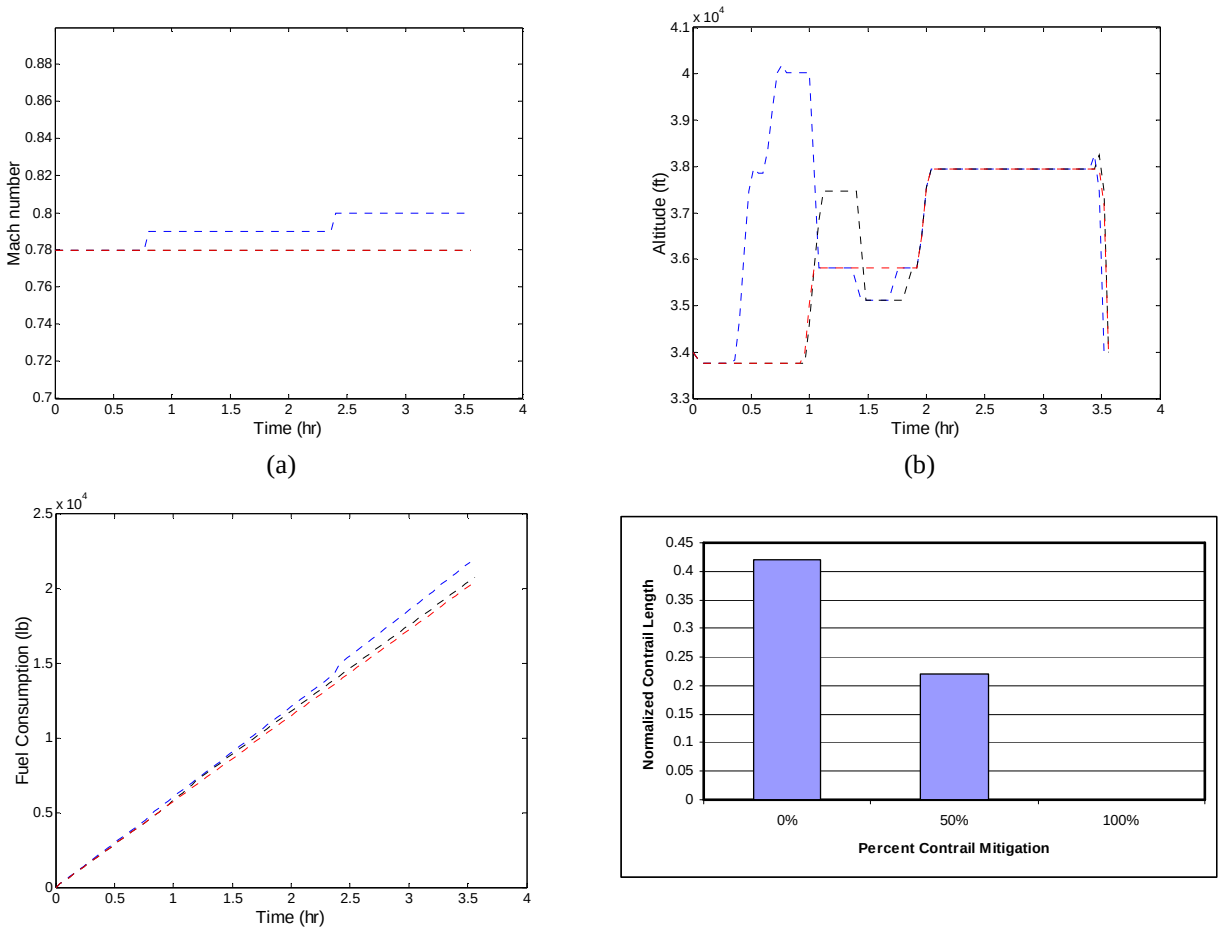

Fig 8. Aircraft performance: (a) velocity time history, (b) altitude time history, (c) fuel burn time history, (d) persistent contrail formation bar graph

Table 4 Comparison of receding horizon trajectory performance

	Contrail Penalty 0%	Contrail Penalty 50%	Contrail Penalty 100%
Max. Velocity	454.1 knots	454.1 knots	467.3 knots
Avg. Velocity	450.6 knots	450.6 knots	464.8 knots
Total Fuel Burn	20,431 lbs	20,734 lbs	21,695 lbs
Flight Time	3.55 hrs	3.55 hrs	3.60 hrs
Normalized Contrail Length	0.42	0.22	0.00

VI. Conclusions

This paper presented a new strategy to mitigate the formation of persistent contrails. Unlike previous research studies using RH-MILP for path planning, this work penalized flight through an obstacle instead of precluding it. The benefit of penalizing flight through an area of RHi > 100% instead of precluding it is that in some cases strict avoidance of contrail formation is very costly in terms of fuel consumption, as was seen in previous work.[11] In addition to the operational benefits, this method also allows analysis of the tradeoff between persistent contrail mitigation and increased fuel consumption. A comparison of the computation time to solve the optimizations with

hard and soft constraints was negligible. Also, due to the scale of the dynamics of the contrail fields, the receding horizon approach easily accommodated dynamic RHi contours with little added computational complexity.

Acknowledgments

The authors would like to thank Marcia Politovich, Frank McDonough, and Gary Cunning of The National Center for Atmospheric Research for their help in obtaining the atmospheric data used in this paper. The authors would also like to acknowledge the support given to this work by a NASA GSRP fellowship.

References

[1]Waitz, I., Townsend, J., Cutcher-Gershenfeld, J., Greitzer, E., and Kerrebrock, J. *Report to the United States Congress: Aviation and the Environment, A National Vision, Framework for Goals and Recommended Actions*. Partnership for AiR Transportation Noise and Emissions Reduction, MIT, Cambridge, MA, 2004.

[2]Intergovernmental Panel on Climate Change, *Aviation and the Global Atmosphere*. J. E. Penner, D. H. Lister, D. J. Griggs, D. J. Dokken, and M. McFarland (eds.), Cambridge University Press. Cambridge, UK, 1999.

[3]Wuebbles, D, et. al. *Workshop on the Impacts of Aviation on Climate Change: A Report of Findings and Recommendations*. Cambridge, MA, June 7-9, 2006.

[4]Travis, D. J., Carleton, A. M., and Lauritsen, R. G., "Contrails reduce daily temperature range," Nature. Vol 418. 8 August 2002. p. 601.

[5]Next Generation Air Transportation System, Federal Aviation Administration Report to the U.S. Congress, 2004.

[6]Noland, R. B., and Williams, V., "Policies for Mitigating Contrail Formation from Aircraft," *Proceedings of the AAC-Conference*, AAC, Friedrichshafen, June 2003, pp. 328-333.

[7]Williams, V., and Noland, R. B., "Variability of Contrail Formation Conditions and the Implications for Policies to Reduce the Climate Impacts of Aviation," *Transportation Research Part D*, Vol. 10, No. 4, 2005, pp. 169-280.

[8]Fichter, C., Marquart, S., Sausen, R., and Lee, D. S., "The Impact of Cruise Altitude on Contrails and Related Radiative Forcing," *Meteorologische Zeitschrift*, Vol. 14, No. 4, Aug. 2005, pp. 563-572.

[9]Mannstein, H., Spichtinger, P., and Gierens, K., "A Note on How to Avoid Contrail Cirrus," *Transportation Research Part D*, Vol. 10, No. 5, 2005, pp. 421-426.

[10]Klima, K., "Assessment of a Global Contrail Modeling Method and Operational Strategies for Contrail Mitigation," M.S. Thesis, MIT, 2005.

[11]Campbell, S., Neogi, N., and Bragg, M., "An Optimal Strategy for Persistent Contrail Avoidance," AIAA Guidance, Navigation, and Control Conference and Exhibit, Honolulu, Hawaii, Aug. 18-21, 2008.

[12]Bryson, A. E., and Ho, Y, C., *Applied Optimal Control*, Taylor and Francis, Levittown, PA, 1975.

[13]Frazzoli, E., "Robust Hybrid Control for Autonomous Vehicle Motion Planning," PhD Dissertation, MIT, 2001.

[14]Milan, M., "Real-Time Optimal Trajectory Generation for Constrained Dynamical Systems," PhD Dissertation, Cal Tech, 2003.

[15]Schouwenaars, T., "Safe Trajectory Planning for Autonomous Vehicles," PhD Dissertation, MIT, 2005.

[16]Kuwata, Y., "Trajectory Planning for Unmanned Vehicles using Robust Receding Horizon Control," PhD Dissertation, MIT, 2007.

[17]Bellingham, J., Richards, A., and How, J. P., "Receding Horizon Control of Autonomous Aerial Vehicles," Proceedings of the IEEE American Control Conference, May 2002, pp. 3741-3746.

[18]Kuwata, Y., and How, J. P., "Three Dimensional Receding Horizon Control for UAVs," Proceedings of the AIAA Guidance, Navigation, and Control Conference, Aug 2004. AIAA-2004-5144.

[19]Culligan, K., "Nap of the Earth Trajectory Design using MILP," M.S. Thesis, MIT, 2006.

[20]Schouwenaars, T., Feron, E., de Moor, B., and How, J. P., "Mixed Integer Programming for Multi-vehicle Path Planning, " Proceedings of the European Control Conference, European Union Control Association, Porto, Portugal, September, 2001, pp. 2603-2608.

[21]Ma, C. S., and Miller, R. H., "Mixed Integer Linear Programming Trajectory Generation for Autonomous Nap-of-the-Earth Flight in a Threat Environment," IEEE Aerospace Conference, 2005.

[22]Chaudhry, A., Misovec, K., and D'Andrea, R., "Low Observability Path Planning for an Unmanned Air Vehicle Using Mixed Integer Linear Programming," *43rd IEEE Conference on Decision and Control*, Paradise Island, Bahamas, Dec. 14-17, 2004.

[23]United States Environmental Protection Agency. "Aircraft Contrails Factsheet," EPA430-F-00-005, September 2000.

[24]Duda et al, "CONUS Contrail Frequency Estimated for RUC and Flight Track Data," European Conference on Aviation, Atmosphere, and Climate, June 30-July 3, 2003.

[25]Burkhardt, U., Karcher, B., Mannstein, H., and Schumann, U., "Climate impact of contrails and contrail cirrus," Aviation Climate Change Research Initiative (ACCRI), Jan. 25, 2008.

[26]Gierens, K., Spichtinger, P., "On the size distribution of ice supersaturated regions in the upper troposphere and lowermost stratosphere," Ann. Geophys., 18 (2000) 1687-1690.

[27]Spichtinger, P., Gierens, K., Leiterer, U., and Dier, H., "Ice supersaturation in the tropopause region over Lindenberg, Germany," Meteor. Z., 12 (2003) 143-156.

[28]Spictinger, P., Gierens, K., and Read, W., "The global distribution of ice-supersaturated regions as seen by the microwave limb sounder," Q. J. R. Meteorol. Soc. 129, 3391-3410, 2003.

[29]Gettleman, A., Fetzer, E. J., Eldering, A., and Irion, F. W., "The global distribution of saturation in the upper troposphere from the Atmospheric Infrared Sounder," *J. Clim*. 19, 6089-6103, 2006.

[30]Gierens, K., Schumann, U., Helten, M., Smit, H., and Marenco, A., "A distribution law for relative humidity in the upper troposphere and lower stratosphere derived from three years of MOZAIC measurements," *Ann. Geophys.* 17, 1218-1226, 1999.

[31]Gibson, J. K., Kallberg, P., Uppala, S., Hernandez, A., Nomura, A., and Serrano, E., "ERA Description," *ECMWF Re-Analysis Project Report Series*, 1, 1-72, 1997.

[32]Benjamin, S. G., D. Devenyi, S. S. Weygandt, K. J. Brundage, J. M. Brown, G. A. Grell, D. Kim, B. E. Schwartz, T. G. Smirnova, T. L. Smith, and G. S. Manikin, "2004: An hourly assimilation/forecast cycle: The RUC," Mon. Wea. Rev., 132, 495-518 (Feb. issue).

[33]Yoder, T., "Development of Aircraft Fuel Burn Modeling Techniques with Applications to Global Emissions Modeling and Assessment of the Benefits of Reduced Vertical Separation Minimums," M.S. Thesis, MIT, 2007.

[34]Jardin, M. R., "Ideal Free Flight through Multiple Aircraft Neighboring Optimal Control," *Proceedings of the American Control Conference*, Chicago, IL, June, 2000, pp. 2879-2885.

[35]Roskam, J., *Airplane Design, Part IV: Preliminary Calculation of Aerodynamic, Thrust and Power Characteristics*, DARcorporation, Lawrence, KS, 2000.

[36]Anderson, J. D., *Aircraft Performance and Design*, McGraw-Hill, 1999.

[37]PERF: Engine Performance Analysis Program v4.2

[38]Lambert, M., Munson, K., Taylor, M, J, H., and Taylor, J. W. R., (eds.) *JANES'S ALL THE WORLD AIRCRAFT*, Jane's Information Group, Alexandria, VA, 1990.

[39]Padilla, C. E., *Optimizing Jet Transport Efficiency*, McGraw-Hill, 1996.

[40]ILOG, *ILOG CPLEX User's guide*, 2007.